Journal of Pharmaceutical and Biomedical Analysis 247 (2024) 116251

Contents lists available at ScienceDirect

Journal of Pharmaceutical and Biomedical Analysis

journal homepage: www.journals.elsevier.com/journal-of-pharmaceutical-and-biomedical-analysis

Integrated serum pharmacochemistry, network pharmacology, and pharmacokinetics to clarify the effective components and pharmacological mechanisms of the proprietary Chinese medicine Jinkui Shenqi Pill in treating kidney yang deficiency syndrome

Jinwei Gao [a,b], Enyu Xu [c], Hongjin Wang [d], Lin Wang [a], Shuoyu Chen [b], Chongji Wang [b], Fanhao Meng [a,*]

[a] School of Pharmacy, China Medical University, Shenyang 110122, China
[b] School of Pharmacy, Shenyang Medical College, Shenyang 110034, China
[c] School of Forensic Medicine, China Medical University, Shenyang 110122, China
[d] School of Pharmacy, Shenyang Pharmaceutical University, Shenyang 110016, China

ARTICLE INFO

Keywords:
Proprietary Chinese medicine Jinkui Shenqi Pill
Kidney yang deficiency syndrome
Serum pharmacochemistry
Network pharmacology
Pharmacokinetics

ABSTRACT

The proprietary Chinese medicine Jinkui Shenqi Pill (PCM-JKSQP) is a classic compound used for the effective clinical treatment of kidney yang deficiency syndrome (KYDS), a metabolic disease accompanied by kidney injury. However, its active ingredients and therapeutic mechanisms are not clear. This study employed serum pharmacochemistry, network pharmacology, and pharmacokinetics (PK) to identify the bioactive components of PCM-JKSQP and preliminarily clarify its mechanism in treating KYDS. One hundred and forty chemical components of PCM-JKSQP, 47 (20 parent compouds and 27 metabolites) of which were absorbed into the blood, were identified by ultra-high-performance liquid chromatography-quadrupole-orbitrap high-resolution mass spectrometry (*UHPLC-Q-Orbitrap HRMS*). The topological parameters of network pharmacology and high concentrations in blood found six parent components as PK markers (cinnamic acid, paeonol, loganin, morroniside, apigenin, and poricoic acid A). PK analysis further identified these six compounds as active ingredients. Protein-protein interaction (PPI) analysis and molecular docking simulation predicted and verified eight core targets (TP53, ESR1, CTNNB1, EP300, EGFR, AKT1, ERBB2, and TNF). Most were concentrated in the MAPK, HIF-1, and PI3K-AKT signaling pathways, indicating that these six active ingredients may mainly exert therapeutic effects through these three pathways via their core targets. The PK results also showed these six components were absorbed quickly, although cinnamic acid and paeonol were rapidly metabolized, with a short half-life and retention time. Loganin and morroniside did not have high peak concentrations, and apigenin and poricoic acid A had long retention times. This study provides a new overall perspective for exploring the bioactive components and mechanisms underlying the effects of PCM-JKSQP in treating KYDS.

1. Introduction

Kidney yang deficiency syndrome (KYDS) is closely related to factors such as body yang deficiency, elderly kidney deficiency, and prolonged illness [1]. When the levels of body yang qi are diminished, the transpiration and gasification of essential qi in the kidney become weak, leading to disorders of water metabolism. Clinical features, such as weak waist and knees, frequent nocturia, and the increased production of clear urine, are common. Therefore, KYDS has been proposed to be related to pathological changes in the kidney based on traditional Chinese medicine (TCM) theory and modern medical research [2]. Thus, an effective and classical KYDS model was established in rats by the intragastric administration of high doses of adenine, which precipitates in the renal tubules, resulting in chronic renal failure, and the clinical features of KYDS, to investigate this hypothesis [3].

The proprietary Chinese medicine Jinkui Shenqi Pill (PCM-JKSQP) was developed on the basis of the Shenqi Pill in the Synopsis of the Golden Chamber and the modified Shenqi Pill in Jisheng Prescription,

* Corresponding author.
E-mail address: fhmeng@cmu.edu.cn (F. Meng).

https://doi.org/10.1016/j.jpba.2024.116251
Received 29 December 2023; Received in revised form 16 May 2024; Accepted 19 May 2024
Available online 22 May 2024

which is composed of 10 TCMs (*Ramulus cinnamomi*, *Aconite*, *Rehmannia glutinosa*, *Corni fructus*, *Poria cocos*, *Moutan cortex*, *Alismatis rhizoma*, *Rhizoma dioscoreae*, *Plantaginis semen*, and *Achyranthes bidentata*) [4]. PCM-JKSQP, which functions by warming the kidney yang, transforming qi, and improving water flow, is mainly used to treat conditions such as edema caused by kidney deficiency, weak waist and knees, inhibited urination, and chilly limbs [5,6]. In modern clinical applications, the prescription is used to treat chronic bronchial asthma, nephritis, renal failure, and prostatitis, as well as adrenocortical dysfunction, and conditions such as diabetes, hypothyroidism, and Alzheimer's disease [7,8]. PCM-JKSQP fully reflects the multi-system, multi-target, multi-channel mode of action and treatment characteristics of TCM. However, the active compounds, potential targets, and pathways of this prescription involved in the mechanism underlying the therapeutic effects of PCM-JKSQP on KYDS remain to be identified by systematic analysis.

Network pharmacology is used to systematically analyze the network of interactions between drugs, targets, and diseases. It is an approach that highlights instances of synergy and is consistent with the mechanism of action of TCM [9,10]. However, this method generally focuses on the *in vitro* composition of the drug without considering its *in vivo* composition and metabolites that are absorbed into the blood. Serum pharmacochemistry is used to identify the substances absorbed into the blood, including parent compouds and metabolites, and may have therapeutic effects [11]. Pharmacokinetics (PK) is employed to study the continuous transformation process of bioactive ingredients to further reveal therapeutic substances [12]. Therefore, combining serum pharmacochemistry and PK analysis with network pharmacology provides a comprehensive approach to the discovery of bioactive compounds and their interactions with targets to identify the pharmacodynamic material basis and mechanism of action of TCM prescriptions.

This study established a sensitive ultra-high-performance liquid chromatography-quadrupole-orbitrap high-resolution mass spectrometry (UHPLC-Q-Orbitrap HRMS) method to detect the parent compouds and metabolites absorbed into the blood of rats. Network pharmacology and pathway enrichment analysis were employed to screen the key parent compouds and underlying mechanisms. The active ingredients were predicted based on topological parameters and high levels *in vivo*. The core targets of the active ingredients were then predicted by protein-protein interaction (PPI) analysis and verified by molecular docking simulation. Finally, UHPLC-Q-TRAP-MS/MS was used to quantify the bioactive compounds and analyze the PK characteristics of the core compounds.

2. Materials and methods

2.1. Chemicals and reagents

Acteoside, loganin, morroniside, sweroside, paeonol, gallic acid, protocatechuic acid, cinnamaldehyde, paeoniflorin, quercetin, apigenin, cinnamic acid, and poricoic acid A reference standards (purity $\geq$ 98 %) were obtained from Baojichenguang Herbpurify (Baoji, China). Liquid-chromatography mass spectroscopy (LC-MS)-grade formic acid, acetonitrile, and methanol were obtained from Fisher Scientific (Fair Lawn, NJ, USA). All other reagents were analytical grade. The proprietary Chinese medicine Jinkui Shenqi Pill was manufactured by Beijing Tong Ren Tang Group (Batch No. 19032638, Beijing, China).

2.2. Animals

All animal experiments conducted in this study were approved by the Experimental Animal Ethics Committee of Shenyang Medical College, China (Approval Number: SYYXY2021082001). Male Sprague-Dawley rats (250 $\pm$ 10 g) were purchased from Changsheng Biotechnology Co., Ltd. (Benxi, China) and maintained under specific pathogen-free conditions at 22 ℃-24 ℃ and 55 %-65 % relative humidity under 12 h light and dark photoperiods. Animals were used in experiments after one week of adaptive feeding.

2.3. Serum pharmacochemical analysis

2.3.1. Biological sample collection and pretreatment

Rats were randomly allocated to administration and blank groups (n = 6 per group). The administration group received 2.0 g/kg/d PCM-JKSQP intragastrically for one week, while the blank group received an equal volume of normal saline. Before the last intragastric administration, the rats were fasted for 12 h, with free access to water. Orbital blood samples (0.5 mL) were collected into heparin sodium tubes at 0, 0.5, 1, 1.5, 2, 3, 4, 8, 12, and 24 h after the last intragastric administration. The samples were mixed and centrifuged (3,000 r/min) for 10 min at 4 ℃. Plasma was collected and stored at -80 ℃ prior to analysis.

Plasma samples from each time point were mixed in equal proportions. An aliquot (200 μL) of the biological samples was treated with 600 μL methanol and vortexed for 5 min to precipitate the proteins. After centrifugation (12,000 rpm) for 10 min, the supernatants were collected and dried under nitrogen gas at room temperature. The residues were reconstituted in 100 μL of 50 % methanol, vortexed for 3 min, and centrifuged (12,000 rpm) for 10 min before 2 μL was injected into the UHPLC-Q-Orbitrap HRMS system for analysis.

2.3.2. UHPLC-Q-Orbitrap HRMS analysis

The DIONEX UltiMate 3000 UHPLC system with a Q-Exactive Orbitrap tandem mass spectrometer was employed for UHPLC-Q-Orbitrap HRMS detection (Thermo Fisher Scientific, Waltham, MA, USA).

The UHPLC analysis was performed with an ACQUITY UHPLC® BEH C_{18} column (2.1 $\times$ 100 mm, 1.7 μm) maintained at 30 ℃. Samples (2 μL injection volume) were separated using a mobile phase consisting of acetonitrile (A) and 0.1 % formic acid (B) at a flow rate of 0.4 mL/min under the following linear flow gradient: 5 % A at 0–1 min, 5 %-99 % A at 1–7 min, 99 % A at 7–12 min, 99 %-5 % A at 12–13 min, and 5 % A at 13–15 min.

The mass spectrometry conditions were based on a heated electrospray ionization source (ESI) operated in positive and negative ion modes under the following operating parameters: auxiliary flow rate, 10 arb; sheath flow rate, 30 arb; capillary temperature, 320 °C; spray voltage, 3.8 kV; and auxiliary gas heater temperature, 350 °C. The first-order full-scan mass spectrum was obtained from *m/z* 100–1,500 with a resolution of 70,000, while the secondary mass spectra were acquired at a resolution of 17,500 with collision energies (CEs) of 15, 30, and 60 eV.

2.3.3. Data processing

An internal database that included the compound name, chemical formula, and molecular weight of the PCM-JKSQP chemical components was established. First, the established database was screened for potential candidate compounds with a matching molecular formula and accurate relative molecular weight error within 5 parts per million. Then, compounds were identified by comparison with reference substances. Raw data from the plasma samples in the administration and blank groups were imported into Xcalibur software and processed using the "background subtract" mode to obtain accurate molecular weights for the potential parent components and metabolites. The parent components absorbed in rats were screened by comparison with the *in vitro* components of PCM-JKSQP. The *m/z* values of the fragment ions of each metabolite were compared with the *m/z* values of the corresponding parent components to locate the metabolic sites in certain regions of the molecule and predict the possible metabolite structures. Finally, the main metabolites of PCM-JKSQP were determined by comparing the retention time, accurate mass, and fragment ions with those reported in the literature.

Table 1
The optimal MRM quantification parameters of six analytes and IS.

Name	t_R (min)	Precursor ion	Product ion	Declustering potential(V)	Collision energy (eV)
Morroniside	2.26	451.2 [M+HCOO]-	243.1	-60	-25
Loganin	2.77	435.1 [M+HCOO]-	227.0	-60	-23
Cinnamic acid	4.90	147.1[M-H]-	103.1	-40	-15
Apigenin	4.98	269.1[M-H]-	117.1	-134	-45
Paeonol	5.54	165.1[M-H]-	122.1	-75	-29
Poricoic acid A	7.26	497.3[M-H]-	423.3	-40	-45
Acetylsalicylic acid	3.86	179.0[M-H]-	137.0	-20	-14

2.4. Network pharmacological analysis

2.4.1. Construction and analysis of the components-targets-pathways network

First, the parent components screened by serum pharmacochemical methods were input into the PubChem (https://pubchem.ncbi.nlm.nih.gov/; PubChem 2023) database to obtain 2D structures and canonical SMILES before the targets of the compounds were predicted using the PharmMapper (https://www.lilab-ecust.cn/pharmmapper/; PharmMapper 2017) and Swiss Target Prediction (https://www.swisstargetprediction.ch/; SwissTargetPrediction 2019) databases. The UniProt (https://www.uniprot.org/; Uniprot 2023) database was used to standardize the gene names of the targets. Subsequently, disease targets were searched in the Therapeutic Target Database (http://db.idrblab.net/ttd/; TTD 2023), DrugBank (https://go.drugbank.com/; DrugBank 6.0), DisGeNET (https://www.disgenet.org/; V 7.0), and GenAge (https://genomics.senescence.info/genes/human; Gen 2018) disease databases, using "edema," "aging," "chronic nephritis," "diabetic nephropathy," and "chronic kidney disease" as keywords. Duplicate targets were deleted. Finally, common targets were identified by comparing the predicted targets of these compounds with those of diseases.

The common targets were imported into DAVID (https://david.ncifcrf.gov/; David 2021) for gene ontology (GO) function and Kyoto Encyclopedia of Genes and Genomes (KEGG) pathway enrichment analyses ($P \leq 0.05$). A components-targets-pathways (CTP) network based on components, targets, and KEGG pathways was constructed using Cytoscape. Topologic analysis was performed to screen for key potential active compounds and pathways with degree values of $\geq 2 \times$ the degree median, betweenness centrality (BC), and closeness centrality (CC) of $\geq 1 \times$ the median. Among these components, the core components with high concentrations in blood were identified as PK markers.

2.4.2. Core target screening and molecular docking simulation

For core target screening, the targets of the core components for treating KYDS were imported into the String (https://string-db.org/; String 2023) database, and the species was defined as "*Homo sapiens*." The minimum required interaction score was no less than 0.9, while the free target was removed. PPI information was then obtained and imported into Cytoscape. Topological analysis was performed using the CytoHubba plug-in, and the top eight targets with the highest degree were displayed in clusters and identified as the core targets.

Molecular docking of the core components and core target molecules was simulated using the Schrodinger Small Molecule Drug Discovery Suite (Schrodinger 2018). The structures of the core compounds were drawn, and the energy was minimized using ChemDraw3D. The protein file was downloaded from the Research Collaboratory for Structural Bioinformatics Protein Data Bank (https://www.rcsb.org/; PDB 2023), and a series of modifications, such as removing water molecules and ligands, hydrotreating, balancing charges, and forming binding pockets, were performed to complete docking analysis. Generally, a chemical binding energy of < -5 kcal/mol was used as the threshold for stable binding. Finally, the docked compounds and proteins were visualized using PyMOL.

2.5. Pharmacokinetic study

2.5.1. Plasma sample collection and preparation

Eight rats were fasted for 12 h before administration. After fasting for 12 h, PCM-JKSQP was administered to rats (n = 8) by intragastric gavage at a dose of 2.0 g/kg, which was equivalent to twice the clinical dosage used in humans. Orbital blood samples (0.5 mL) were collected into heparin sodium tubes from the ophthalmic vein at 0, 0.083, 0.25, 0.5, 0.75, 1, 1.5, 2, 3, 4, 8, 12, 24, and 36 h after intragastric administration. Plasma was immediately obtained by centrifugation (3,000 r/min) for 10 min at 4 ℃ and stored at -80 ℃ until analysis.

Sample (100 μL), 10 μL of internal standard (IS) working solution, and 300 μL of methanol were mixed in a 2-mL Eppendorf tube to precipitate the proteins and vortexed for 2 min, followed by sonication for 15 min. After centrifugation (12,000 rpm) for 10 min, the supernatant was transferred to another Eppendorf tube and evaporated to dryness under nitrogen at 37 ℃. The residue was reconstituted with 100 μL of 50 % methanol, vortexed for 2 min, sonicated for 3 min, and centrifuged (12,000 rpm) for another 10 min. Finally, the supernatant (10 μL) was injected into the UHPLC-MS/MS system for analysis.

2.5.2. Preparation of calibration standard and quality control samples

The six reference substances were dissolved in methanol to prepare stock solutions at the following final concentrations: morroniside, 210.0 μg/mL; loganin, 125.0 μg/mL; cinnamic acid, 243.0 μg/mL; apigenin, 183.0 μg/mL; paeonol, 210.0 μg/mL; and poricoic acid A, 208.0 μg/mL. Serial dilutions of the standard stock solutions were made with methanol. Acetylsalicylic acid was used as the IS and prepared at a concentration of 1.80 μg/mL in methanol. Calibration standards were prepared after adding 10 μL of the working solutions to 100 μL of blank rat plasma. The following calibration standards were prepared by serial dilution: morroniside at 2.1, 8.4, 16.8, 42, 105, 262.5, 525, and 1050 ng/mL; loganin at 1.25, 5, 10, 25, 62.5, 156.25, 312.5, and 625 ng/mL; cinnamic acid at 2.43, 9.72, 19.44, 48.60, 121.5, 303.75, 607.5, and 1215 ng/mL; apigenin at 1.83, 7.34, 14.64, 36.6, 91.5, 228.75, 457.5, and 915 ng/mL; paeonol at 2.1, 8.4, 16.8, 42, 105, 262.5, 525, and 1050 ng/mL; and poricoic acid A at 2.08, 8.32, 16.64, 41.6, 104, 260, 520, and 1040 ng/mL. Quality control (QC) samples were prepared at low, medium, and high concentrations as follows: morroniside at 6.3, 63, and 630 ng/mL; loganin at 3.75, 37.5, and 375 ng/mL; cinnamic acid at 7.29, 72.9, and 729 ng/mL; apigenin at 5.49, 54.9, and 549 ng/mL; paeonol at 6.3, 63, and 630 ng/mL; and for poricoic acid A at 6.24, 62.4, and 624 ng/mL.

2.5.3. UHPLC-Q-TRAP-MS/MS analysis

The ExionLC™ AD UHPLC system coupled with an AB SCIEXQ-TRAP® 5500 tandem mass spectrometer (AB SCIEX, Framingham, MA, USA) was employed for UHPLC-Q-TRAP-MS/MS analysis. The mobile phase consisted of A (0.1 % formic acid) and B (acetonitrile) with a gradient elution (0–4 min 5 %-40 % B; 4–5 min 40 %-60 % B; 5–8 min 60 %-95 % B; 8–8.5 min 95 %-5 % B; and 8.5–10 min 5 % B) at a flow rate of 0.4 mL/min. The mass spectrometer was equipped with an ESI under the following conditions: curtain gas, 35 L/min; collision gas, medium/9; turbo ion spray voltage, −4500 eV; temperature, 550 ℃; ion source gas 1, 50 L/min; and ion source gas 2, 55 L/min. Details of the optimized transitions, CE, and declustering potential collected by multiple reaction monitoring in the negative ion mode are shown in Table 1.

2.5.4. Method validation

The selectivity, carryover, linearity and lower limit of quantification (LLOQ), accuracy and precision, extraction recovery and matrix effect, and stability of the method were validated according to the Bioanalytical Method Validation Guidelines (Chinese Pharmacopoeia 2020, Vol. 4).

Table 2
The parent components and metabolites of proprietary Chinese medicine Jinkui Shenqi Pill (PCM-JKSQP) in rat plasma sample.

No.	t_R (min)	Formula	Observed *m/z* (Error/ppm)	MS/MS fragmentations	Identification	Source	species	Type
1	0.70	$C_7H_{12}O_6$	191.0553[M-H]$^-$ (1.5)	173.0086, 111.0074	quinic acid	F	phenolic acids	P1
2	0.72	$C_4H_6O_5$	133.0131[M-H]$^-$ (-0.2)	115.0024, 71.0124	malic acid	D	phenolic acids	P2
3	0.91	$C_5H_5N_5$	136.0615[M+H]$^+$ (-3.9)	119.0351, 107.0490	adenine	F	purines	P3
4	0.92	$C_6H_8O_7$	191.0189[M-H]$^-$ (1.4)	173.0087, 129.0181	citric acid	C	organic acids	P4
5	0.93	$C_{15}H_{22}O_{10}$	407.1179 [M+COOH]$^-$ (2.5)	361.1155, 199.0605, 151.0390	catalpol	C	iridoid glycosides	P5
6	0.99	$C_5H_8O_5$	147.0288[M-H]$^-$ (-0.1)	129.0181, 87.0074	malic acid methyl ester	D	phenolic acids	P6
7	1.24	$C_8H_8O_4$	167.0339[M-H]$^-$ (-0.8)	149.0201, 123.0429	vanillic acid	E	phenolic acids	P7
8	1.65	$C_9H_{11}O_2N$	166.0857[M+H]$^+$ (-1.0)	120.0301, 121.0311, 149.0608, 131.0506	hydration product of gentianine lost CO	D	alkaloids	M1
9	1.90	$C_6H_6O_3$	127.0387[M+H]$^+$ (-3.7)	109.0283, 97.0285	5-HMF	C, D	furan derivatives	P8
10	2.19	$C_9H_{10}O_8S$	277.0024[M-H]$^-$ (4.3)	197.0411, 182.0242	dimethylation and sulfate conjugation of gallic acid	D	phenolic acids	M2
11	2.52	$C_{16}H_{22}O_{10}$	373.1134[M-H]$^-$ (1.2)	211.0607, 167.0703, 149.0597, 123.0439	swertiamarin	D	iridoid glycosides	P9
12	2.58	$C_8H_{10}O_6S$	233.0124[M-H]$^-$ (4.3)	153.0511, 123.0452	hydroxytyrosol sulfate conjugation	C	organic alcohol	M3
13	2.82	$C_9H_{12}O_6S$	247.0279[M-H]$^-$ (3.2)	167.0706, 153.0469, 123.0446	methylated hydroxytyrosol sulfate conjugation	C	organic alcohol	M4
14	2.94	$C_9H_8O_2$	147.0441[M-H]$^-$ (0.1)	119.0490, 102.9475	cinnamic acid	B	organic acids	P10
15	2.98	$C_{17}H_{26}O_{10}$	435.1491 [M+COOH]$^-$ (3.5)	389.1467, 227.0921, 127.0388, 101.0231	loganin	D	iridoid glycosides	P11
16	3.03	$C_{17}H_{26}O_{11}$	451.1455 [M+COOH]$^-$ (1.1)	405.1407, 243.0873, 155.0341, 101.0232	morroniside	D	iridoid glycosides	P12
17	3.09	$C_7H_6O_2$	121.0283[M-H]$^-$ (-1.0)	102.6190	benzoic acid	E	organic acids	P13
18	3.12	$C_{14}H_{16}O_9$	327.0724[M-H]$^-$ (3.5)	175.0224, 151.0326, 113.0201, 85.0311	demethylated and paeonol glucuronide conjugation	E	organic phenols	M5
19	3.16	$C_9H_{10}O_7S$	261.0086[M-H]$^-$ (2.8)	181.0502, 166.0313, 138.0333, 123.0112	hydroxylated and paeonol sulfate conjugation	E	organic phenols	M6
20	3.18	$C_{10}H_{10}O_7S$	273.0086[M-H]$^-$ (8.4)	193.0501, 149.0521	methylated caffeic acid sulfate conjugation	C	phenolic acids	M7
21	3.21	$C_9H_9O_3N$	178.0501[M-H]$^-$ (1.7)	134.0604	alkene to ketone and glycination of cinnamic acid	B	organic acids	M8
22	3.35	$C_9H_8O_6S$	242.9964[M-H]$^-$ (0.2)	163.0393, 119.0509	hydroxylation and sulfate conjugation of cinnamic acid	B	organic acids	M9
23	3.38	$C_7H_6O_7S$	233.0124[M-H]$^-$ (3.0)	153.0501, 109.0605	sulfate conjugation of protocatechuic acid	B	phenolic acids	M10
24	3.34	$C_{15}H_{18}O_9$	341.0884[M-H]$^-$ (2.3)	165.0582, 151.0344	paeonol glucuronide conjugation	E	organic phenols	M11
25	3.43	$C_8H_8O_7S$	246.9918[M-H]$^-$ (4.8)	167.0311, 151.0012	methylation and sulfate conjugation of protocatechuic acid	B	phenolic acids	M12
26	3.53	$C_7H_6O_4$	153.0183[M-H]$^-$ (-0.2)	109.0282, 81.0334	protocatechuic acid	B	phenolic acids	P14
27	3.57	$C_8H_8O_3$	151.0390[M-H]$^-$ (0)	135.0102, 109.0312,	demethylated paeonol	E	organic phenols	M13
28	3.62	$C_9H_{10}O_6S$	245.0124[M-H]$^-$ (1.5)	165.0582, 151.0344	paeonol sulfate conjugation	E	organic phenols	M14
29	3.78	$C_{10}H_{10}O_7S$	273.0041[M-H]$^-$ (0.2)	193.0451, 149.0611, 134.0363	sulfate conjugation of ferulic acid	H	phenolic acids	M15
30	3.79	$C_{11}H_{19}N_3O_2$	224.1402[M-H]$^-$ (3.9)	141.0910	plantagoguanidinic acid A	I	alkaloids	P15
31	4.01	$C_7H_6O_3$	137.0233[M-H]$^-$ (0)	93.0305, 65.0425	dedihydroxylation of gallic acid	B	phenolic acids	M16
32	4.06	$C_{15}H_{10}O_5$	269.0458[M-H]$^-$ (4.8)	117.0104	apigenin	I	flavonoids	P16
33	4.10	$C_9H_{16}O_4$	187.0968[M-H]$^-$ (-1.1)	125.0960	azelaic acid	D	organic acids	P17
34	4.13	$C_{10}H_{14}O_6S$	261.0440 [M-H]$^-$ (4.6)	181.0903 166.0302, 137.1002	sulfated pinane	E	monoterpenoid	M17
35	4.39	$C_9H_{10}O_7S$	261.0076[M-H]$^-$ (4.9)	181.0862, 137.0961	dimethylation and sulfate conjugation of protocatechuic acid	B	phenolic acids	M18
36	4.41	$C_9H_{14}O_5$	201.0742[M-H]$^-$ (-7.4)	153.0320, 139.1102, 121.0603	hydrogenation product of catalpol aglycone	C	iridoid	M19
37	4.66	$C_{11}H_{18}O_5$	229.1051[M-H]$^-$ (-8.7)	185.1355, 142.9951, 116.7811	hydrogenated loganetin	D	iridoid	M20

(*continued on next page*)

Table 2 (*continued*)

No.	t_R (min)	Formula	Observed *m/z* (Error/ppm)	MS/MS fragmentations	Identification	Source	species	Type
38	4.70	$C_8H_8O_5$	183.0297[M-H]$^-$ (5.4)	153.0107, 139.0406	methylation of gallic acid	D	phenolic acids	M21
39	4.90	$C_9H_{10}O_4$	181.0864[M-H]$^-$ (3.0)	137.1012	dimethylation of protocatechuic acid	B	phenolic acids	M22
40	4.94	$C_{11}H_{16}O_5$	227.0921[M-H]$^-$ (3.1)	209.1201, 183.1411, 165.1265, 127.0388	loganetin	D	iridoid	M23
41	5.02	$C_{10}H_{14}O_6$	229.0711[M-H]$^-$ (1.3)	211.1315, 183.1021, 167.1416	methylation and hydroxylation product of catalpol aglycone	C	iridoid	M24
42	5.17	$C_{13}H_{18}O_7$	285.2072[M-H]$^-$ (-3.4)	243.1105, 155.1401, 141.1301	acetylated morronisid aglycone	D	iridoid	M25
43	5.46	$C_9H_{14}O_4$	185.0818[M-H]$^-$ (5.4)	166.9901, 141.1312, 123.0804	dehydroxylation and hydrogenation products of catalpol aglycone	C	iridoid	M26
44	5.49	$C_{11}H_{14}O_4$	209.0814[M-H]$^-$ (3.4)	190.9989, 165.1265	dehydrated loganetin	D	iridoid	M27
45	5.50	$C_9H_{10}O_3$	165.0547[M-H]$^-$ (0.3)	150.0312, 135.0078, 122.0362, 108.0443	paeonol	E	organic phenols	P18
46	6.78	$C_{31}H_{46}O_5$	497.3283[M-H]$^-$ (4.2)	423.2913, 211.1492	poricoic acid A	F	Triterpenic acid	P19
47	7.05	$C_{31}H_{48}O_4$	483.3487[M-H]$^-$ (3.7)	481.3301, 421.3131	dehydrotumulosic acid	F	Triterpenic acid	P20

Notes: A-*Aconite*, B-*Ramulus cinnamomi*, C-*Rehmannia glutinosa*, D-*Corni fructus*, E-*Moutan cortex*, F-*Poria*, G-*Alismatis rhizoma*, H-*Achyranthes bidentata*, I-*Plantaginis semen*

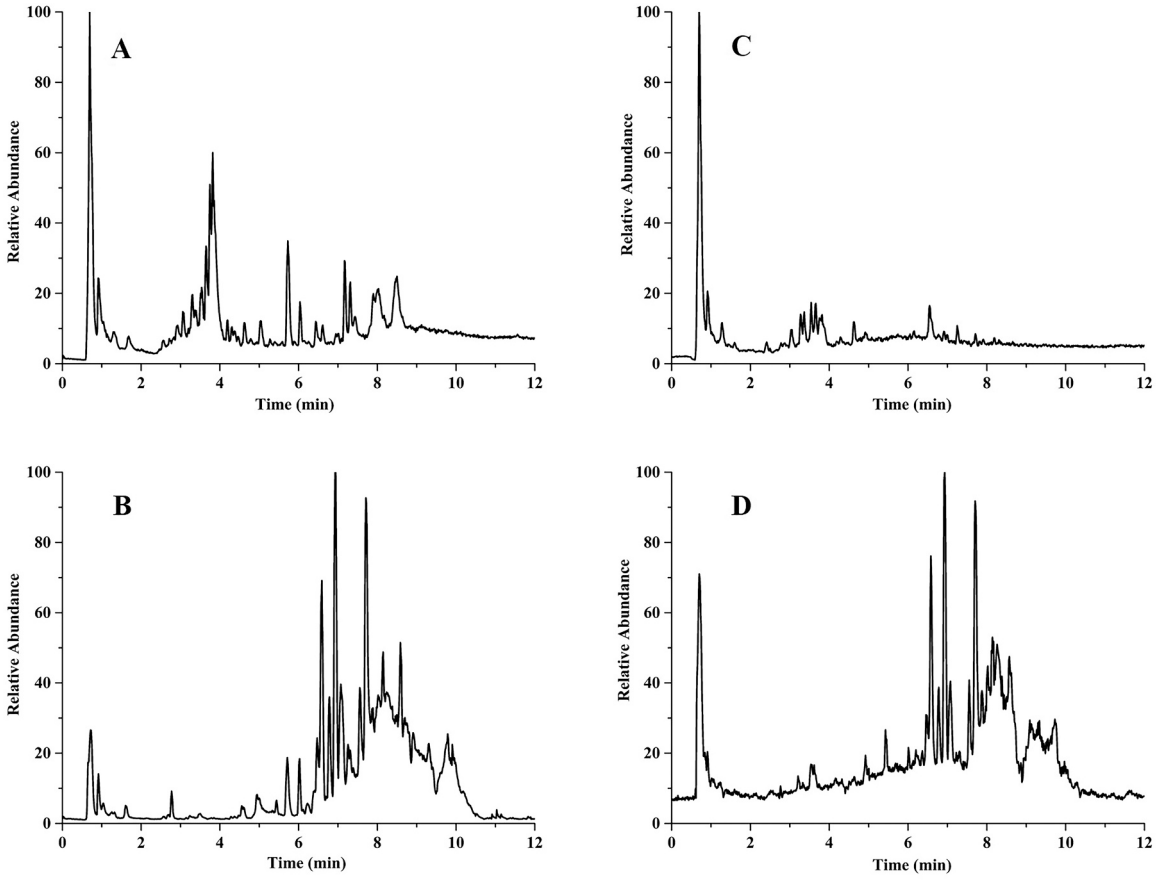

Fig. 1. Total ion chromatograms (TICs) of the PCM-JKSQP in positive/negative ion mode (A/B), the rat plasma sample after oral administration of PCM-JKSQP in positive/negative ion mode (C/D).

Selectivity can determine whether the established method can distinguish the target analyte and IS from the endogenous components of the matrix. The plasma of six rats was mixed and used as a blank substrate. A simulated plasma sample was prepared by taking 10 μL of the mixed reference solution, blowing it to dryness, and adding 100 μL of blank substrate. Blank plasma, simulated plasma samples, and plasma samples taken after PCM-JKSQP administration were pretreated as described (Section 2.5.1) and injected for analysis. The Chinese Pharmacopoeia (ChP) stipulates that the response of an interfering component has to be less than 20 % of the LLOQ response and less than 5 % of the IS response.

A standard curve was made from a series of simulated plasma samples with concentration gradients, with duplicates of each concentration treated in parallel. The ratio of the chromatographic peak area (Y)

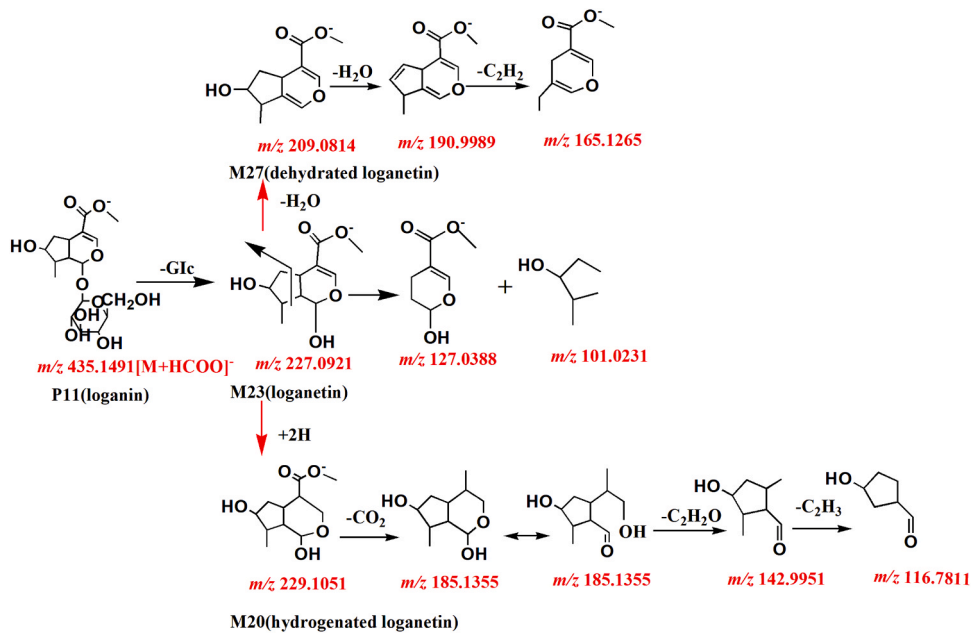

Fig. 2. Proposed fragmentation pathways of P11, M20, M23, M27.

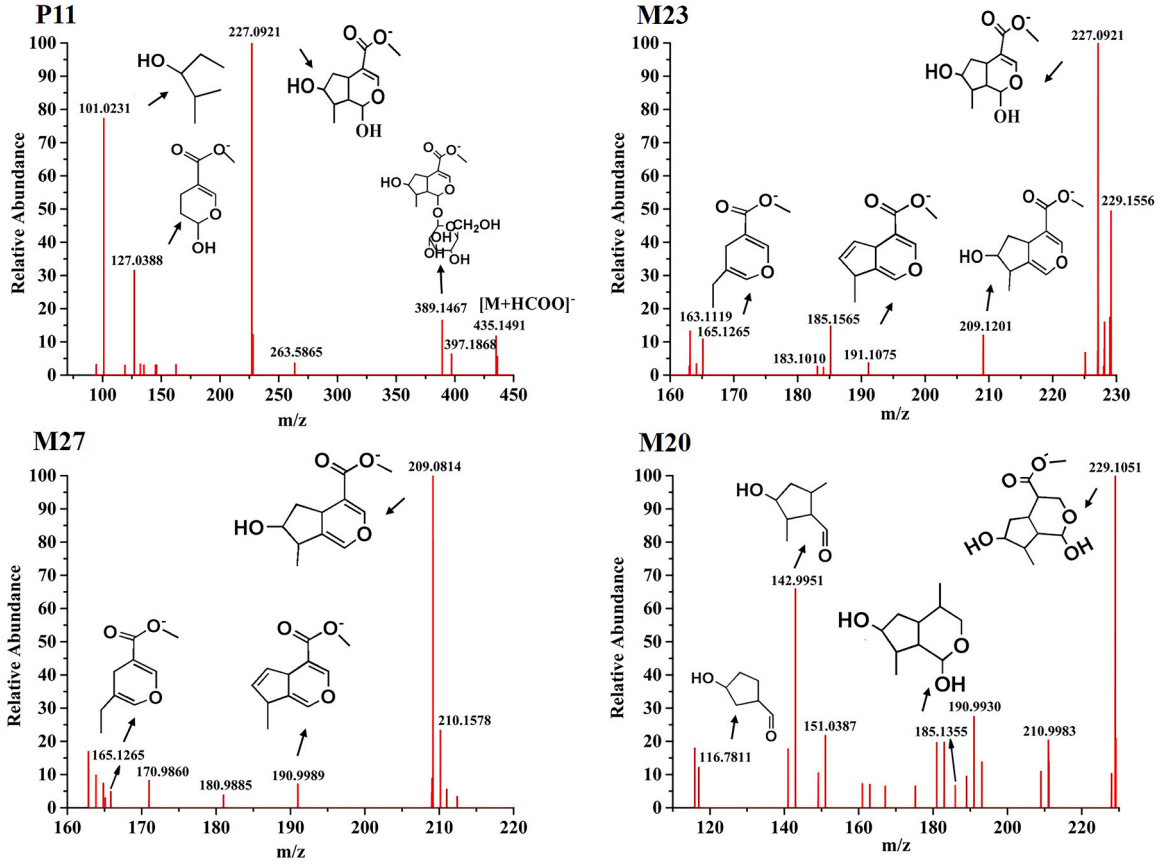

Fig. 3. MS/MS spectrums of P11, M20, M23, M27.

between the drug and the IS was plotted on the Y-axis and the sample concentration (X) on the X-axis to obtain the corresponding regression equation. The ChP stipulates that the correlation coefficient (r) is required to be > 0.99.

The lower limit of quantification (LLOQ) was obtained by analyzing six replicates of plasma samples at the lowest concentration on the calibration curve and the relative standard deviation (RSD) value was required to be less than 20 %.

Four concentrations (LLOQ, low, medium, and high) of QC samples were prepared, and six replicates of each concentration were processed in parallel over three consecutive days. The concentration of the tested substance in the plasma sample was calculated according to the

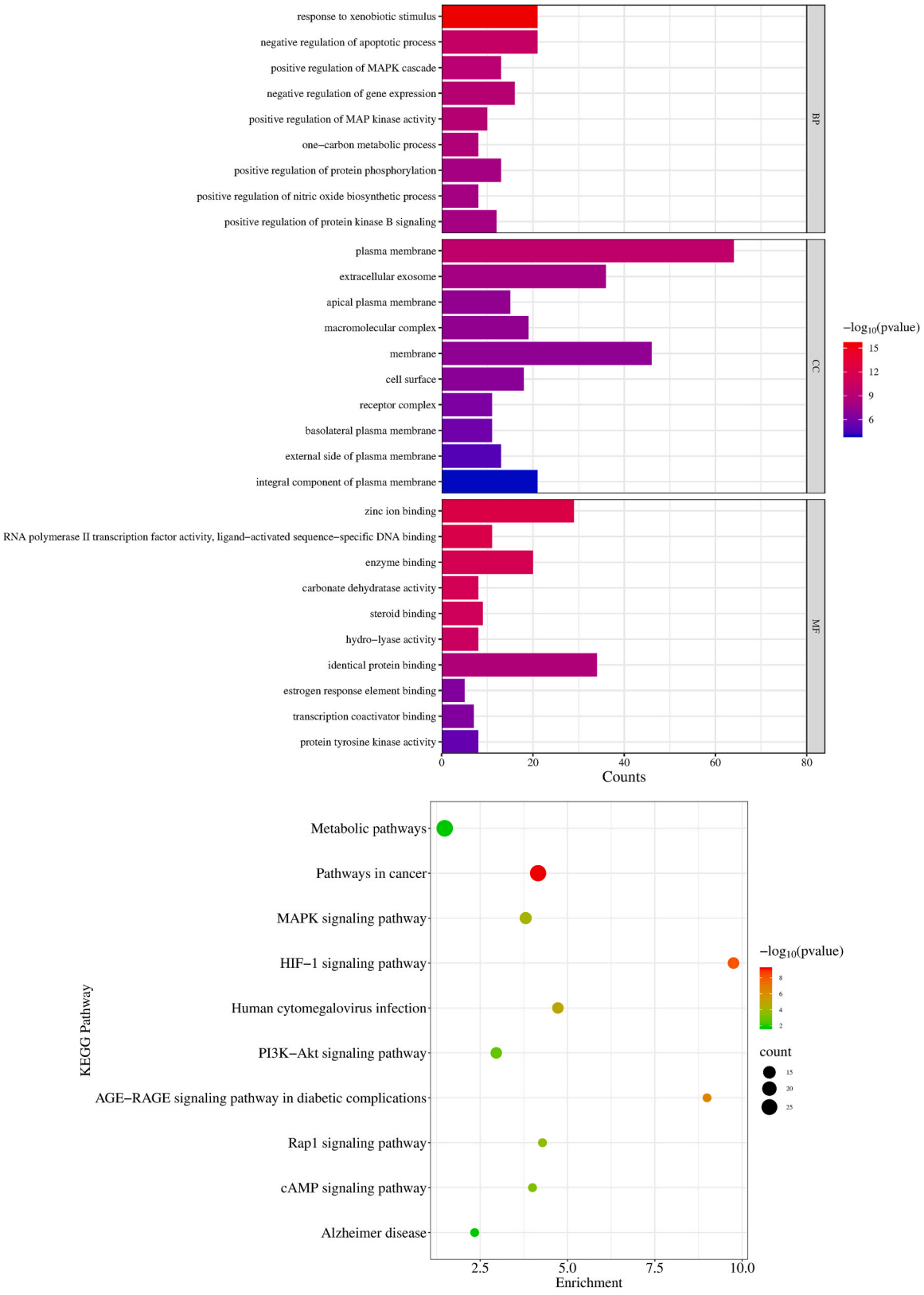

Fig. 4. Network pharmacology analysis of PCM-JKSQP on KYDS: (A) GO enrichment analysis; (B) KEGG pathway analysis; (C) The network diagram of "components-targets-pathways" (The V-shaped, diamond-shaped, and ellipse-shaped nodes represented pathways, serum migrating components, and targets, respectively.); (D) The PPI network and cluster analysis of the disease targets by CytoNCA.

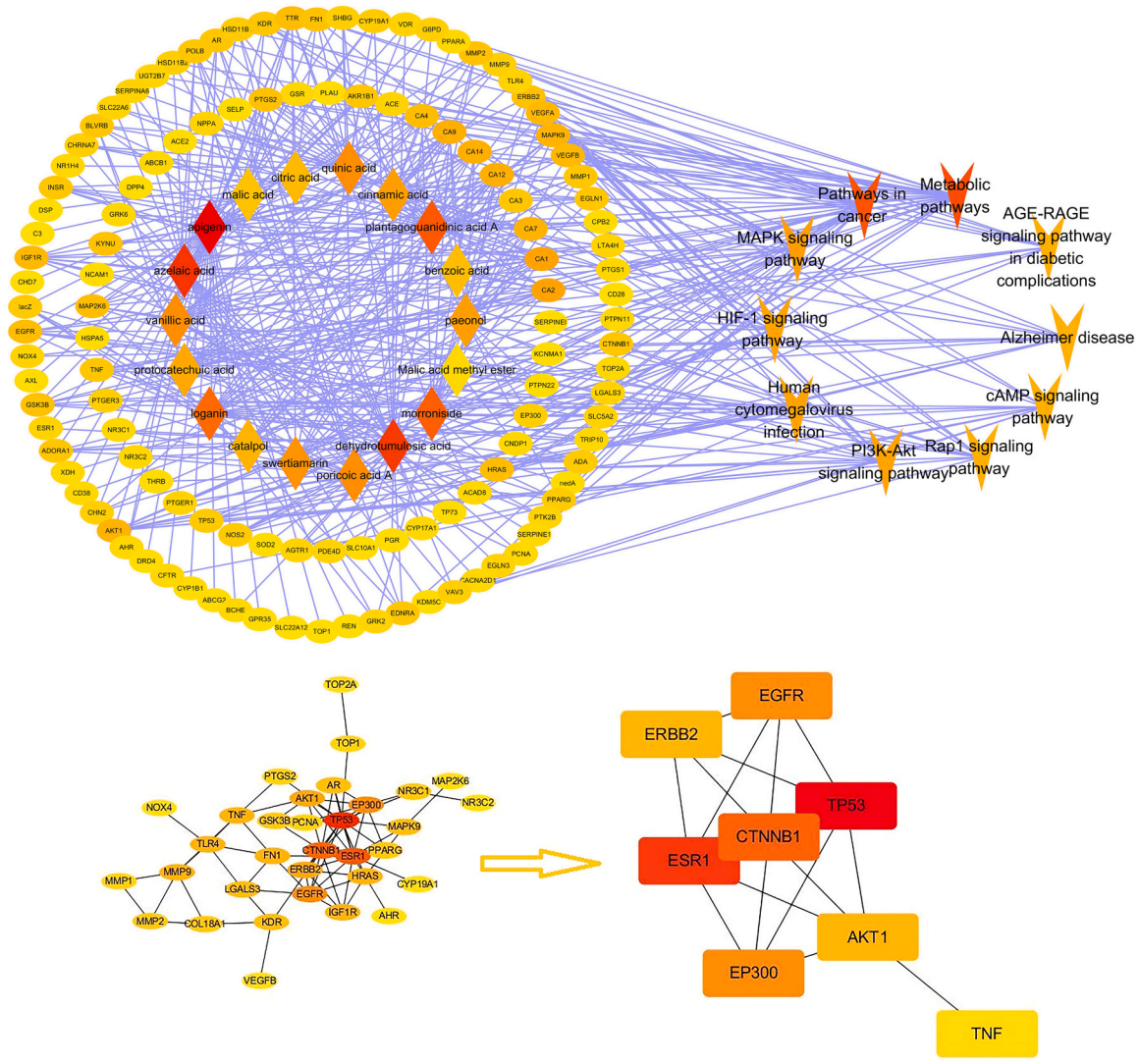

Fig. 4. (*continued*).

accompanying standard curve of each batch, and the precision and accuracy within and between batches were calculated. The RSD value for precision was required to be less than 15 %, and the deviation of accuracy should not have exceeded ± 15 %.

The extraction recovery and matrix effect were determined by QC samples at low-, medium- and high-concentrations. The peak area ratio between the measured component and the IS was marked as A. Another 100 μL of blank plasma sample was treated to obtain supernatant as described (Section 2.5.1). The supernatant was added to the reference solution and IS, dried by nitrogen gas and redissolved. The peak area ratio was calculated using the same method and marked as B. The peak area ratio of the corresponding amount of the reference product and IS solution was calculated by the same method and marked as C. The extraction recovery and matrix effect were determined by the extraction recovery formula: (A/B) × 100 %, and the matrix effect formula: (B/C) × 100 %. The ChP stipulates that the extraction recovery should be greater than 50 %, the matrix effect should be between 85 % and 115 %, and the RSD value of both should be less than 15 %.

Three replicate low-, medium-, and high-concentration QC samples were prepared and placed at -4 ℃ for 24 h before sampling analysis to investigate stability. QC samples were also frozen at -20 ℃ for 12 h, then thawed at room temperature. The process was repeated three times and tested to investigate freeze-thaw stability. Samples were placed at -20 ℃ for 30 days and measured after treatment to investigate long-term stability. The measured results had to meet precision (RSD ≤ 15 %) and accuracy (RE ≤ ± 15 %) requirements to be considered stable.

2.6. Statistical analysis

DAS 3.0 (BioGuider Co., Shanghai, China) was employed to calculate the pharmacokinetic parameters of the analytes. All data were expressed as mean ± SD of six parallel measurements.

3. Results

3.1. Identification of parent components and metabolites in rat plasma

A total of 140 compounds in PCM-JKSQP were identified and preliminarily characterized *in vitro*. These consisted of 21 alkaloids, 22 iridoid glycosides, 12 phenylethanol glycosides, 28 triterpenoids and triterpenoid glycosides, 11 monoterpenoid glycosides, 14 phenolic acids, 10 organic acids/phenols, five flavonoids, eight glycosides, three nucleosides, and six other types. The details of these compounds are shown in Table S1. Based on these results, 47 exogenous substances (20 parent components and 27 metabolites) were identified in plasma collected from rats following the intragastric administration of PCM-JKSQP. The details of these parent components and metabolites are listed in Table 2. The total ion chromatograms (TICs) are shown in Fig. 1.

Table 3
The topological parameters of 13 potential active compounds and 6 top pathways obtained through the network of "components-targets-pathways".

Nodes	Degree	Betweenness Centrality	Closeness Centrality
Apigenin*	42	0.226	0.443
Azelaic acid	32	0.140	0.413
Dehydrotumulosic acid	31	0.131	0.393
Plantagoguanidinic acid A	26	0.137	0.402
Morroniside*	25	0.066	0.391
Loganin*	23	0.050	0.389
Quinic acid	17	0.032	0.355
Vanillic acid	17	0.034	0.377
Poricoic acid A*	17	0.045	0.369
Swertiamarin	16	0.036	0.366
Cinnamic acid*	14	0.021	0.360
Paeonol*	14	0.041	0.373
Protocatechuic acid	12	0.022	0.343
Metabolic pathways	28	0.101	0.393
Pathways in cancer	27	0.075	0.395
MAPK signaling pathway	14	0.017	0.357
HIF-1 signaling pathway	13	0.020	0.360
Human cytomegalovirus infection	13	0.016	0.357
PI3K-Akt signaling pathway	13	0.014	0.360

Notes: Average Degree: 6.392; Average Betweenness Centrality: 0.014; Average Closeness Centrality: 0.336; *: PK markers;

The parent components consisted of one alkaloid, four iridoid glycosides, five phenolic acids, two triterpenic acids, five organic acids/aldehydes/phenols, one flavonoid, and two other types. The retention time of P11 was at t = 2.98 min, the chemical formula was $C_{17}H_{26}O_{10}$, and the quasi-molecular ion peak was at *m/z* 435.1491 $[M+COOH]^-$ or *m/z* 389.1467 $[M-H]^-$ in the negative ion mode. The fragment ions were at *m/z* 227.0921 $[M-H-Glc]^-$, *m/z* 127.0388 $[M-H-Glc-C_6H_{12}O]^-$, and *m/z* 101.0231 $[M-H-Glc-C_4H_{14}O_4]^-$. This compound was identified as loganin, a typical iridoid glycoside, based on a comparison with the reference substance. Three metabolites related to loganin, namely M20, M23, and M27, were detected in the plasma, mainly in phase I metabolism of glucose removal, dehydration, and hydrogenation. The quasi-molecular ion peak of M23 in the negative ion mode was *m/z* 227.0921 $[M-H]^-$, which was 162 Da smaller than that of loganin. The cleavage pattern of M23 was similar to that of loganin. This metabolite was speculated to be an aglycone produced by the removal of glucose from loganin. The excimer ion peak of M20 was 2 Da more than that of M23, while the excimer ion peak of M27 was lower than that of M23 by 18 Da. Based on previous reports [13], these two metabolites were speculated to be hydrogenated loganetin and dehydrated loganetin. The cleavage process and mass spectrogram of the parent component and metabolites are shown in Figs. 2 and 3, respectively.

The $[M-H]^-$ ion of parent compound P14 was 153.0183. After the loss of CO_2 fragments, *m/z* 109.0283 was formed, and characteristic ions, such as *m/z* 81.0334, were generated. Based on a comparison with the reference substance, this compound was identified as protocatechuic acid, a typical representative of phenolic acids, and M10, M12, M18, and M22 were identified as related metabolites. The molecular ion peak of M10 was *m/z* 233.0124 $[M-H]^-$, which was 80 Da higher than that of P14, and the fragment ions generated were the same as those of protocatechuic acid. Therefore, M10 was identified as the sulfated product of protocatechuic acid. The molecular ion peak of M22 was 28 Da higher than that of protocatechuic acid, and only the decarboxylated fragment ion 137.1012 $[M-H-CO_2]^-$ was detected, suggesting that this metabolite was the dimethylation product of protocatechuic acid. The molecular ion peak of M18 was 80 Da higher than that of M22, and fragment ions *m/z* 181.0862 and 137.0961 were generated, suggesting that this metabolite was the sulfated product of M22. Data on the metabolites of protocatechuic acid were consistent with previous reports [14].

The $[M-H]^-$ ion of compound P18 was *m/z* 165.0547, and its fragment ions were *m/z* 150.0312 $[M-H-CH_3]^-$, *m/z* 135.0078 $[M-H-2CH_3]^-$, and *m/z* 122.0362 $[M-H-COCH_3]^-$. Comparison with the reference substance identified paeonol, a typical organic phenol. M5, M6, M11, M13, and M14 were identified as its metabolites, produced in metabolic reactions mainly involving demethylation, hydroxylation, sulfation, and glucuronic acid [15]. Compared with paeonol, the molecular ion peaks of metabolites M11 and M14 were 176 Da and 80 Da higher, respectively, and had the same fragment ions. These compounds were speculated to be glucuronidation and sulfation products of paeonol, respectively. The molecular ion peak of metabolite M13 was 14 Da less than that of paeonol, suggesting that it was the demethylation product of paeonol. This was confirmed by secondary fragment ions at *m/z* 135.0102 $[M-H-O]^-$ and *m/z* 109.0282 $[M-H-C_2H_2O]^-$. The molecular ion peak of metabolite M5 was 176 Da higher than that of M13, and *m/z* 175.0224 ions of glucuronic acid and an *m/z* 151.0390 fragment ion of M5 were observed. Therefore, M5 was speculated to be the glucuronidation product of M13. The metabolic process is shown in Figure S1.

The $[M-H]^-$ ion of compound P19 was *m/z* 497.3283, and its typical fragment ion was *m/z* 423.2913 $[M-H-CH_3CH_2COOH]^-$. This compound was identified as poricoic acid A, a typical triterpenoid acid, based on a comparison with the reference substance.

Acteoside is a representative phenylethanol glycoside. Although this parent compound was not detected in plasma, the metabolites M3, M4, and M7 related to this compound were identified. Hydroxytyrosol and caffeic acid are produced by the metabolism of acteoside [16]. The quasi-molecular ion peak of hydroxytyrosol was *m/z* 153.0511 $[M-H]^-$, and the fragment ion *m/z* 123.0452 $[M-H-CH_2O]^-$ was produced. The $[M-H]^-$ ion of metabolite M3 was 80 Da higher than that of hydroxytyrosol, and *m/z* 153.0511 and *m/z* 123.0452 fragment ions were produced. Therefore, M3 was speculated to be the sulfated product of hydroxytyrosol. Both the excimer ion peak and fragment ion of metabolite M4 were 14 Da higher than that of M3. Therefore, M4 was speculated to be the methylation product of M3. The quasi-molecular ion peak of caffeic acid was *m/z* 179.0339 $[M-H]^-$, and a fragment ion of *m/z* 135.0802 was generated. The fragment ion of metabolite M7 was 14 Da more than that of caffeic acid, and its molecular ion peak was 94 Da ($-SO_3+CH_2$) more than that of caffeic acid. Thus, M7 was assumed to be a methylated caffeic acid sulfate conjugate. The metabolic pathway is shown in Figure S2.

3.2. Network pharmacology study of PCM-JKSQP in KYDS

3.2.1. Target screening of PCM-JKSQP in KYDS

A total of 5,297 targets of the 20 migrating components of PCM-JKSQP in rats were identified by screening the PharmMapper and Swiss Target Prediction databases. In addition, 1,187 KYDS-related targets were retrieved from the TTD, DrugBank, DisGeNET, and GenAge databases. Overall, 119 overlapping targets were identified.

The common targets identified were imported into the DAVID database for GO and KEGG enrichment analyses. The top 10 GO enrichment terms ($P \leq 0.05$) in the biological process (BP), molecular function (MF), and cellular component (CC) categories are shown in Fig. 4A. The BP terms included "response to hypoxia and xenobiotic stimulus," "positive or negative regulation of gene expression and apoptotic process," "inflammatory response," and "signal transduction." The MF terms included "transcription coactivator binding," "enzyme," and "steroid binding." The CC terms included "plasma membrane," "macromolecular complex," and "nucleoplasm." The top 10 enriched KEGG pathways presented as bubble plots based on their *P*-values ($P \leq 0.05$) are shown in Fig. 4B. The KEGG pathways mainly included metabolic pathways, signaling pathways, virus infection, and Alzheimer's disease.

3.2.2. Screening of key components and pathways by constructing a C-T-P network

A C-T-P network consisting of 147 nodes (18 compounds, 119

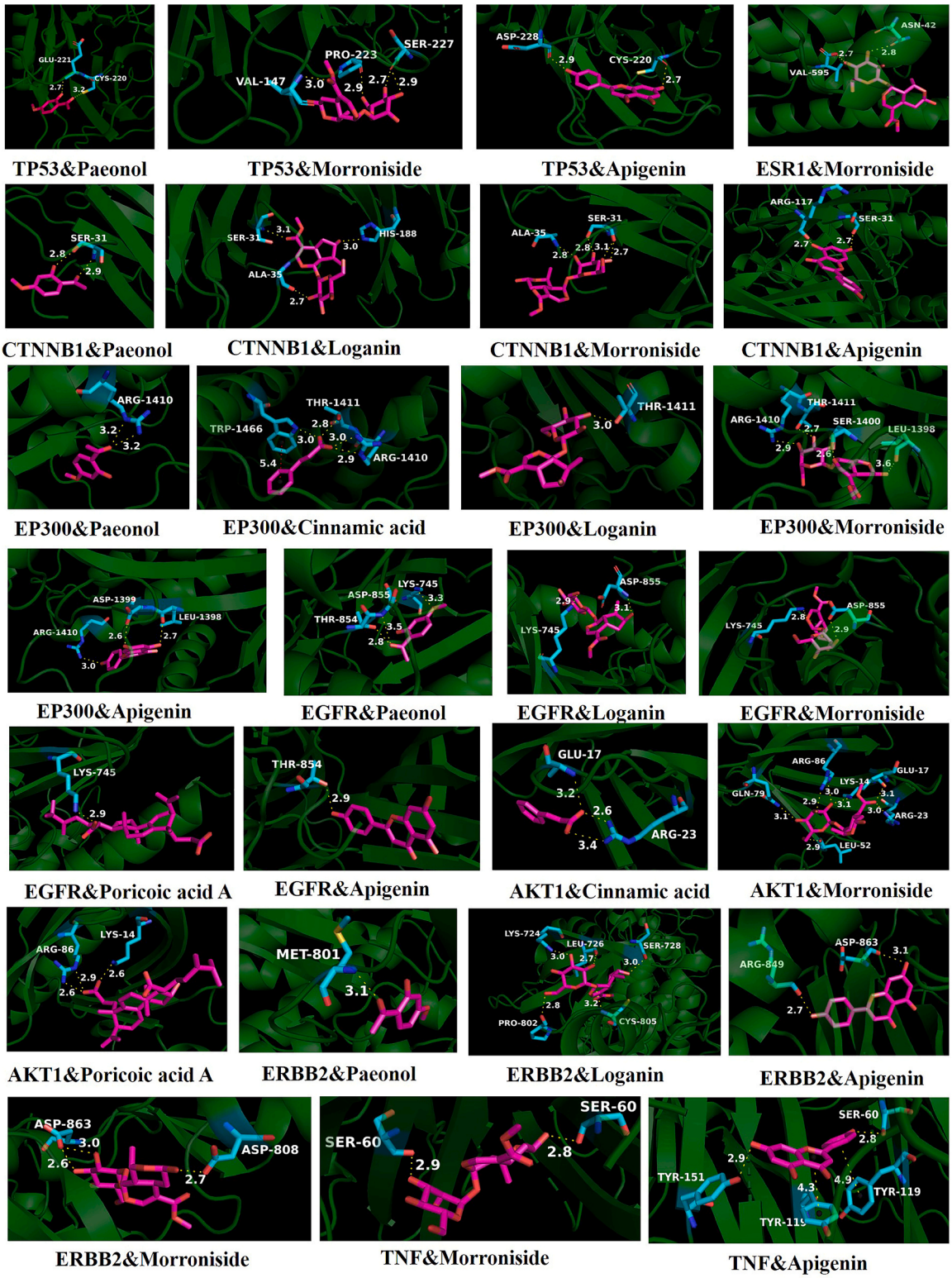

Fig. 5. The conformations of main active compounds and major core targets (binding energies < −5 kcal/mol).

targets, and 10 pathways) and 475 edges (ingredient-target interactions and target-pathway relationships) was generated to explore the active components of PCM-JKSQP against KYDS (Fig. 4C). The Network Analyzer plug-in in Cytoscape was used to calculate the topological parameters. The topological parameters of the 13 compounds were not less than the corresponding medians (Table 3). These compounds were considered to be the main potential compounds active in the effects of PCM-JKSQP on KYDS. Of these, six compounds with high concentrations in the blood were selected as markers for PK analysis and the chemical structures of these compounds are shown in Fig. S3. The top six pathways were also screened according to the topology parameters (Table 3).

3.2.3. *Molecular docking simulation of compounds and targets*

The targets related to the top six active compounds were uploaded to

Table 4
Molecular docking results.

Molecular Target	Docking score (kcal/mol)					
	Loganin	Poricoic acid A	Paeonol	Cinnamic acid	Morroniside	Apigenin
TP53	-4.524	-3.348	-5.696	-3.833	-6.876	-8.161
ESR1	-2.455	-2.249	-4.09	-2.742	-7.865	-4.758
CTNNB1	-6.482	-3.467	-5.197	-3.322	-10.046	-5.378
EP300	-8.18	-4.242	-5.021	-10.331	-10.047	-6.048
EGFR	-7.266	-5.191	-5.420	-3.867	-8.098	-5.311
AKT1	-3.515	-6.79	-4.664	-5.993	-5.615	-3.449
ERBB2	-8.426	-4.289	-6.714	-4.424	-8.582	-7.313
TNF	-7.969	-4.551	-4.392	-3.604	-8.524	-6.175

the String database to predict the PPI network. The top eight core targets were screened for molecular docking simulation using CytoHubba (Fig. 4D). Molecular docking of the six active components with the core targets was simulated to verify the interactions (Fig. 5). In general, lower binding energy between ligands and receptors reflects greater stability of the binding conformation and an increased possibility of interaction. The binding energies of docking between the top eight core targets TP53 (6GGC), ESR1 (7OQB), CTNNB1 (6O9B), EP300 (6V8K), EGFR (7A2A), AKT1 (2UVM), ERBB2 (3PP0), TNF (2AZ5), and the six active components are listed in Table 4. The molecular docking simulation results indicated that most of the binding energies were < -5 kcal/mol, with targets such as TP53, EGFR, AKT1, and ERBB2 exhibiting better binding with the compounds as their binding energies were lower. These proteins were all among the top pathways, including the MAPK, HIF-1, and PI3K-AKT signaling pathways.

3.3. Pharmacokinetic analysis

3.3.1. Method validation

The selectivity of the PK analysis method was assessed by comparing the chromatograms of six different batches of blank plasma samples, blank plasma samples containing mixed reference materials and IS, as well as plasma samples after oral administration. The results confirmed that the endogenous components in the plasma did not interfere with the tested substances. A representative sample chromatogram is shown in Fig. 6.

Carryover of residues was estimated by injecting blank samples following the upper limit of quantification, which should not have exceeded 20 % of the LLOQ and 5 % of the IS. The results showed that the interference at the retention time of the six analytes and IS was negligible.

The linearity of the method was determined using a series of eight standard plasma sample concentrations containing a mixed reference solution added to blank rat plasma. After treatment, the samples were analyzed to record the peak areas of six analytes and the IS. The analytical curves were generated by performing a weighted ($1/x^2$) least square regression on the analyte concentrations (X) versus the peak areas ratio of analytes to IS (Y), the correlation coefficients (r) of which were all > 0.99. The lowest point of the standard curve was the LLOQ of each analyte. Details of the standard curve equations, linear range, and LLOQ of each tested object are shown in Table 5.

The precision and accuracy of the method were determined using QC samples at LLOQ, low, medium, and high concentrations, with six replicates prepared on three consecutive days. The measured concentration was then compared with the declared concentration to examine the intra-day precision (RSD) and accuracy (RE), inter-day precision (RSD) and accuracy (RE) of the method. The results obtained were all < 15 %, which met the relevant requirements (Chinese Pharmacopoeia 2020, Vol. 4) for the determination of biological samples (Table S2).

Extraction recovery was investigated by comparing the mean peak areas of the extracted QC samples with those of the corresponding standard solutions added into the post-extracted blank matrix. The matrix effect was evaluated by comparing the mean peak areas of analytes and the IS dissolved in post-extracted blank matrix with those dissolved in pure solutions. As shown in Table S3, the mean recoveries of the analytes all exceeded 70.28 %, and the matrix effects of the analytes ranged from 95.52 % to 102.49 %, showing that this extraction method met the requirements (Chinese Pharmacopoeia 2020, Vol. 4) for biological sample processing, with no significant matrix effect observed. The RSD value of the recovery and matrix effects were not more than 15 % (Table S3).

The stability of plasma samples stored at -20 °C for 30 days, subjected to three freeze-thaw cycles and placed in a sample injector (4 °C) for 24 h after sample treatment was investigated. The results shown in Table S4 indicated good stability of the six components under these conditions.

3.3.2. Quantitative analysis of the components in PCM-JKSQP

The six components in PCM-JKSQP monitored for PK were subjected to *in vitro* quantitative analysis under the same conditions as those described in the Methods (Section 2.5.3; UHPLC-Q-TRAP-MS/MS analysis). After calculation and conversion, the doses of morroniside, loganin, cinnamic acid, apigenin, paeonol, and poricoic acid A in PCM-JKSQP were 0.58, 0.50, 0.28, 1.40, 2.80, and 74.28 mg/kg, respectively, representing the doses of each component administered to rats.

3.3.3. Pharmacokinetic study

The method developed for PK analysis was applied to investigate the *in vivo* PK of these six absorption components in rats after a single intragastric administration of PCM-JKSQP. The PK parameters and the time-concentration dynamics curves of the six compounds are shown in Table 6 and Fig. 7.

The PK analysis results showed that the plasma concentrations of the six compounds peaked rapidly in rats, with a T_{max} between 30 min and 2 h after the intragastric administration of PCM-JKSQP. The absorption of the compounds was good, with poricoic acid A having the largest area under the curve (AUC). Among these six compounds, the $t_{1/2}$ and $MRT_{0\text{-}t}$ of paeonol were relatively short, and the $t_{1/2}$ and $MRT_{0\text{-}t}$ of apigenin were both longer than those of the other compounds, indicating a longer residence time in the body.

4. Discussion

This study established a systematic method for screening the bioactive compounds of PCM-JKSQP. Compared with the compound information obtained based only on the screening of public databases, that of the parent compounds absorbed into the blood showed a better correlation with the network pharmacological analysis results. More importantly, on this basis, the components with degree values more than twice the mean of the topological parameters and high concentrations in blood were identified as PK markers from among the numerous components absorbed into the blood. PK analysis further identified these six compounds as bioactive ingredients. In addition, investigations into the potential mechanism of the therapeutic effects on KYDS revealed that PCM-JKSQP might act by enriching different hub targets, such as TP53, ESR1, CTNNB1, EP300, EGFR, AKT1, ERBB2, and TNF. The MAPK, HIF-

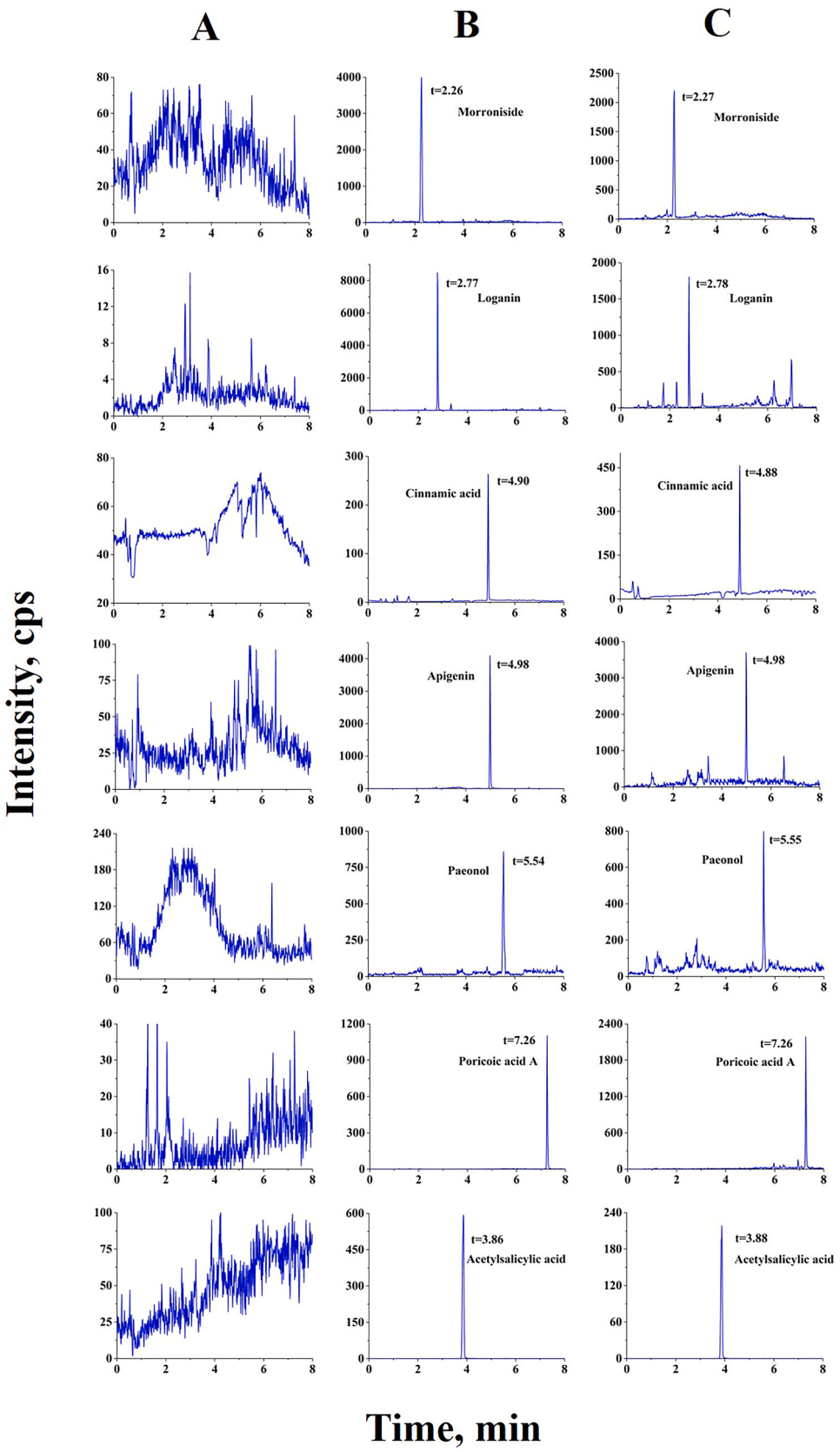

Fig. 6. Multiple reaction monitoring (MRM) chromatograms of the six compounds and IS from rat plasma: A: blank plasma; B: blank plasma spiked with the six analytes and IS; C: real plasma samples obtained from rat after oral administration of PCM-JKSQP.

Table 5
The calibration curves, related coefficients, linear ranges, LLOQs of six analytes.

Analyte	Standard curves	r	Linear ranges (ng/mL)	LLOQs (ng/mL, mean ± SD)	RSD %
Morroniside	y = 0.04653x-0.01019	0.9974	2.10 – 1050.00	2.10 ± 0.15	5.19
Loganin	y = 0.03693x+0.00515	0.9978	1.25 – 625.00	1.25 ± 0.31	7.25
Cinnamic acid	y = 0.01312x+1.22251	0.9973	2.43 – 1215.00	2.43 ± 0.20	5.56
Apigenin	y = 0.31330x+0.16852	0.9965	1.83 – 915.00	1.83 ± 0.28	4.43
Paeonol	y = 0.00852x+0.03091	0.9939	2.10 – 1050.00	2.10 ± 0.39	7.34
Poricoic acid A	y = 0.07371x+0.00429	0.9949	2.08 – 1040.00	2.08 ± 0.83	9.32

1, and PI3K-AKT signaling pathways were identified as the most enriched in the mechanism underlying the effects of PCM-JKSQP on KYDS.

The MAPK signaling pathway has been reported to be involved in kidney function changes through oxidative stress, triggering inflammatory factors and activating inflammatory pathways to cause proteinuria and glomerulosclerosis [17]. MAPK signaling pathway activation can also induce renal proximal tubular epithelial cell apoptosis and promote inflammation to cause renal injury [18]. Hypoxia-inducible factors are key nuclear transcription factors, the subtypes of which not only mediate hypoxia adaptation during renal injury but are also associated with inflammation, epithelial-mesenchymal transition (EMT), and extracellular matrix deposition, thereby participating in fibrotic changes [19]. Podocytes form the outermost layer of the glomerular filtration membrane, which is a key factor in maintaining glomerular function. Podocyte injury leads to disruption of the glomerular filtration barrier. Downregulation of the PI3K/AKT pathway has been shown to reduce podocyte apoptosis [20]. The phosphorylation regulation of the PI3K/AKT signaling pathway regulates a series of downstream effector molecules, which induce different biological functions in renal tissue, including cell death, lipid metabolism, and EMT, thereby leading directly to the progression of renal fibrosis and CKD [21].

Cinnamic acid and cinnamaldehyde are the active components of the monarch drug *Ramulus cinnamomi* in PCM-JKSQP. Cinnamon inactivates the ERK/JNK/p38 MAPK signaling pathway, leading to reduced renal interstitial fibroblast proliferation and hypertrophy [22]. Cinnamaldehyde attenuates cellular senescence in the kidney by inducing PI3K/AKT pathway-mediated autophagy through microRNA-155 downregulation [23]. The absence of cinnamic aldehyde was presumed to be due to its oxidization to cinnamic acid [24]. This study showed that the PK of cinnamic acid followed the two-compartment mode, with rapid absorption and metabolism and short retention time in the body. Although cinnamic acid is metabolized quickly in the blood, it is reported to exert a cumulative effect [25]. After administering multiple doses, the C_{max} of cinnamic acid is approximately two-fold greater than that of a single intragastric dose. However, the mechanism underlying the protective

Table 6
The pharmacokinetic parameters for six analytes in *vivo* after gavage with PCM-JKSQP (n = 6, mean ± SD).

Analyte	AUC_{0-t} (ug/L*h)	$AUC_{0-\infty}$ (ug/L*h)	$t_{1/2}$ (h)	T_{max} (h)	C_{max} (ug/L)	MRT_{0-t} (h)	$MRT_{0-\infty}$ (h)	CLz/F (L/h/kg)
Morroniside	1754.70 ± 347.44	1793.24 ± 356.44	7.48 ± 0.14	1.33 ± 0.26	488.852 ± 18.50	5.69 ± 0.48	6.57 ± 0.51	0.34 ± 0.074
Loganin	1059.53 ± 152.74	1072.33 ± 152.78	6.32 ± 0.38	0.88 ± 0.14	318.67 ± 22.72	6.70 ± 0.24	7.17 ± 0.194	0.48 ± 0.075
Cinnamic acid	1368.19 ± 361.87	1378.69 ± 367.35	3.60 ± 1.39	1.08 ± 0.20	412.20 ± 20.37	4.16 ± 1.18	4.48 ± 1.22	0.21 ± 0.04
Apigenin	4538.19 ± 754.60	4730.03 ± 828.32	7.77 ± 1.37	1.04 ± 0.25	771.24 ± 30.23	8.75 ± 1.14	10.52 ± 1.49	0.303 ± 0.051
Paeonol	698.29 ± 30.40	709.65 ± 32.02	2.19 ± 0.10	0.54 ± 0.10	526.75 ± 29.94	1.76 ± 0.08	1.98 ± 0.11	12.48 ± 0.169
Poricoic acid A	5961.95 ± 1465.92	6158.43 ± 1488.56	7.40 ± 1.49	1.67 ± 0.26	950.26 ± 38.35	8.04 ± 1.09	9.59 ± 1.35	12.7 ± 3.19

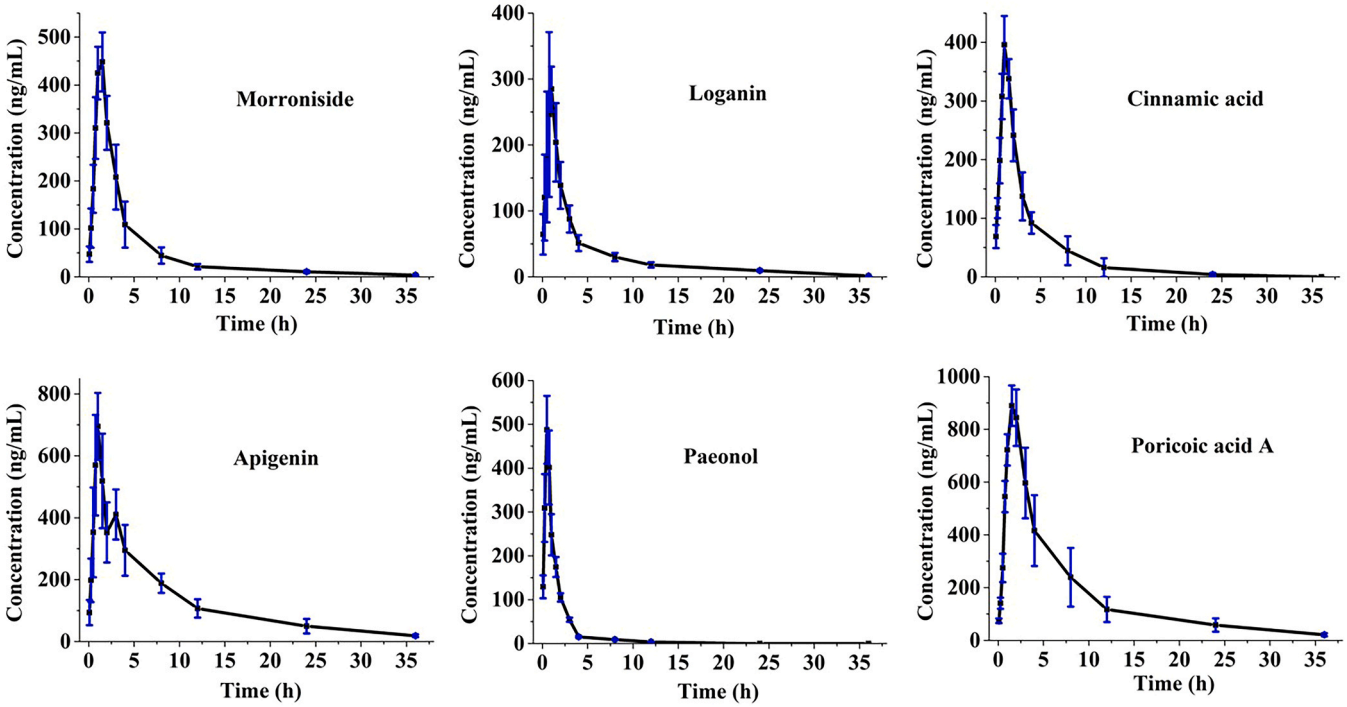

Fig. 7. Mean plasma concentration-time curves of six analytes after oral administration of PCM-JKSQP in rats (mean ± SD, n = 6).

effect of cinnamic acid against kidney disease remains to be elucidated.

Loganin and morroniside, which are kidney-tonifying ingredients found in the minister drug *Corni fructus*, alleviate renal inflammation and damage to the glomerulus and renal interstitium by regulating the p38 MAPK signaling pathway [26]. Loganin alleviates renal injury by regulating tubular epithelial cell apoptosis via the PI3K/AKT signaling pathway [27]. Morroniside reduces podocyte apoptosis by restoring blocked cellular autophagy flux and inhibiting NOX4 overexpression and reactive oxygen species accumulation [28]. Molecular docking simulation showed that loganin and morroniside bound effectively with targets of the PI3K/AKT and MAPK signaling pathways, including EGFR, ERBB2, AKT1, and TP53 (energy values < -5 kcal/mol). According to the PK analysis, these two substances peaked quickly and had a long retention time *in vivo*, although their peak concentrations were not high, suggesting that glycosides are rapidly hydrolyzed to aglycones.

In the PCM-JKSQP prescription, *Poria cocos* and *Plantaginis semen* are used as adjunctive drugs, which clear dampness and promote diuresis. Poricoic acid A is a component of *Poria cocos* that was absorbed quickly, reaching its peak at around 1.6 h, with a long half-life and retention time. Among the six analytes, poricoic acid A had the largest AUC, which may be related to the high content of *Poria cocos* in the prescription. Poricoic acid A was reported to significantly reduce the activation of renal fibroblasts and interstitial fibrosis [29] and inhibit fibrosis by regulating the PDGF-C, Smad3, and MAPK signaling pathways [30]. The PK analysis in this study showed that the *Plantaginis semen*-derived component apigenin had a long retention time in rats and exhibited a double-peak phenomenon. The sulfate conjugate of apigenin is excreted in bile, and high rates of clearance may lead to hepatoenteric circulation, resulting in the persistence of the parent compound in the systemic circulation. Recent studies showed that apigenin had a protective effect on kidney injury in rats [31] and alleviated kidney cell damage by inhibiting oxidative stress and inflammation [32] via a mechanism that may be related to the AGE-RAGE signaling pathway [33]. Paeonol, which is the effective ingredient of *Moutan cortex*, was shown to reduce mesangium [34] and renal interstitium fibrosis [35]. This study found that paeonol was absorbed quickly, reaching a peak approximately 30 min after intragastric administration. The retention time and half-life in rat were short, which may be related to the metabolism of paeonol. Many metabolites of paeonol were identified based on previous metabolic analyses [15].

A limitation of this study should be noted. The core targets identified using the methods established in this study require further validation in animal models of KYDS.

5. Conclusions

Integrated serum pharmacochemistry, network pharmacology, and PK were used in this study to systematically screen the active ingredients of PCM-JKSQP for treating KYDS and preliminarily explore the therapeutic mechanism. A rapid and sensitive UHPLC-Q-Orbitrap HRMS analysis method was established, which was then applied to the successful identification of 140 *in vitro* components and 47 serum migration components as potential therapeutic components of PCM-JKSQP. Six key active ingredients were successfully screened through network pharmacology and PK analysis. Molecular docking simulation suggested that these six bioactive components may primarily exert therapeutic effects through eight core targets that were mainly concentrated in the MAPK, HIF-1, and PI3K-AKT signaling pathways. This study provides a reference for the investigation of the effective components of TCM formulas and their mechanisms of action.

CRediT authorship contribution statement

Hongjin Wang: Supervision, Software, Methodology. **Lin Wang:** Supervision, Project administration. **Jinwei Gao:** Writing – original draft, Visualization, Validation, Software, Methodology, Investigation, Funding acquisition, Formal analysis, Data curation. **Enyu Xu:** Supervision, Resources, Methodology. **Shuoyu Chen:** Visualization, Software. **Chongji Wang:** Visualization, Software. **Fan-hao Meng:** Writing – review & editing, Funding acquisition, Conceptualization.

Declaration of Competing Interest

The authors declare that they have no known competing financial interests or personal relationships that could have appeared to influence the work reported in this paper.

Acknowledgements

This work was financially supported by the Science Research Fund Project of Liaoning Provincial Department of Education (Grant No. JYTMS20231404), and the Young- and Middle-Aged Scientific and Technological Innovation Talents Plan in Shenyang (Grant No. RC200367).

Appendix A. Supporting information

Supplementary data associated with this article can be found in the online version at doi:10.1016/j.jpba.2024.116251.

References

[1] D.W. Chen, Y.C. Meng, X.J. Fang, Q. Huang, Progress and prospect of modern medical research on the nature of kidney yang deficiency syndrome, Mod. J. Integr. Tradit. Chin. West. Med. 14 (2005) 3175–3177.
[2] Y.L. Zhang, C.R. Guo, Z.M. Sun, Advances in the biological basis of kidney yang deficiency syndrome, Chin. J. Tradit. Med. Sci. Technol. 26 (2019) 318–319.
[3] V. Diwan, A. Mistry, G. Gobe, L. Brown, Adenine-induced chronic kidney and cardiovascular damage in rats, J. Pharm. Toxicol. Methods 68 (2013) 197–207.
[4] F.Y. Xu, L.Y. Cao, Discussion on the formula and syndrome of Jinkui Shenqi Pill and its clinical application, Chin. J. Tradit. Chin. Med. Pharm. 30 (2015) 931–932.
[5] J.Z. Lu, L. Zhang, Investigation of the clinical application of Guifu Dihuang Wan and Jingui Shenqi Wan, Chin. J. Tradit. Chin. Med. Pharm. 28 (2013) 2194–2197.
[6] Y.H. Zhao, Z.Y. Gao, C.H. Sun, The Analyses on the Indications and Principal Drugs of Golden Cabinet's Kidney Qi Pill, Chin. J. Exp. Tradit. Chin. Formul. 15 (2009) 112–114.
[7] A.X. Li, R. Xie, Interpretation of the evolution and application of Jinkui Shenqi Pill and its propritary Chinese medicines, J. Tradit. Chin. Med. 19 (2020) 18–23.
[8] Y.E. Wang, X.X. Fu, L.J. Feng, Protective effect and mechanism of Jinkui shenqi Pill on glomerulonephritis in rats, J. Chin. Med. Mater. 42 (2019) 1173–1176.
[9] J.S. Li, Y. Zhang, S.R. Liu, W.J. Li, Y. Sun, H. Cao, S.M. Wang, J. Meng, A network pharmacology integrated pharmacokinetics strategy to investigate the pharmacological mechanism of absorbed components from crude and processed Zingiberis Rhizoma on deficiency-cold and hemorrhagic syndrome, J. Ethnopharmacol. 301 (2023) 115754.
[10] C.S. Liu, T. Xia, Z.Y. Luo, Y.Y. Wu, Y.N. Hu, F.L. Chen, Q.F. Tang, X.M. Tan, Network pharmacology and pharmacokinetics integrated strategy to investigate the pharmacological mechanism of Xianglian pill on ulcerative colitis, Phytomed 82 (2021) 153458.
[11] L. Ren, Q.Y. Li, L.W. Zhang, R.Y. Wang, F. Qin, L.S. Zhao, X.Y. Wei, Z.L. Xiong, Integrated serum pharmacochemistry, network pharmacology and pharmacokinetics to explore bioactive components of Gushudan in the treatment of osteoporosis, J. Chromatogr. B 1225 (2023) 123762.
[12] W. Tang, Y.H. Lu, Drug metabolism and pharmacokinetics in support of drug design, Curr. Pharm. Des. 15 (2009) 2170–2183.
[13] J.H. Tao, M. Zhao, S. Jiang, X.L. Pu, X.Y. Wei, Comparative metabolism of two major compounds in *Fructus Corni* extracts by gut microflora from normal and chronic nephropathy rats *in vitro* by UHPLC-Q-TOF/MS, J. Chromatogr. B 1073 (2018) 170–176.
[14] M. Xu, Z.C. Zhang, G. Fu, S.F. Sun, J.H. Sun, M. Yang, A.H. Liu, J. Han, D. Guo, Liquid chromatography-tandem mass spectrometry analysis of protocatechuic aldehyde and its phase I and II metabolites in rat, J. Chromatogr. B 856 (2007) 100–107.
[15] L.Q. Ding, Z.X. Liu, F. Zhao, G. Bai, L.X. Chen, X.S. Yao, F. Qiu, Isolation and identification of the metabolites of paeonol in human urine, Xenobiotica 242 (2012) 1206–1212.
[16] J.H. Tao, M. Zhao, D.G. Wang, C. Yang, G.T. Chen, X. Zhao, X.L. Pu, S. Jiang, UHPLC-Q-TOF/MS-based screening and identification of two major bioactive components and their metabolites in normal and CKD rat plasma, urine and feces after oral administration of *Rehmannia glutinosa* Libosch extract, J. Chromatogr. B 1001 (2015) 98–106.
[17] Y.J. Cao, Y.M. Zhang, N. Wang, L.C. He, Antioxidant effect of imperatorin from Angelica dahurica in hypertension via inhibiting NADPH oxidase activation and MAPK pathway, J. Am. Soc. Hypertens. 8 (2014) 527–536.

[18] Q. Zhao, Y.G. Wan, C.J. Wang, Q.X. Wei, H.L. Chen, X.J. Meng, Regulatory mechanism of p38 MAPK signaling pathway on renal tissue inflammation in chronic kidney disease and interventional effect of traditional Chinese medicine, China J. Chin. Mater. Med. 37 (2012) 1700–1704.
[19] H. Zhang, R.F. Xu, Z.C. Wang, Contribution of oxidative stress to HIF-1-mediated profibrotic changes during the kidney damage, Oxid. Med. Cell. Longev. 2021 (2021) 1–8.
[20] F. Dan, X.R. Li, Z.Y. Wang, N.N. Gu, S.X. Zhang, C.F. Li, Y. Chen, Z.Q. Ma, R.C. Lin, H.G. Zhang, C.J. Zhao, Integrated UHPLC-MS and network pharmacology approach to explore the active components and the potential mechanism of Yiqi Huoxue decoction for treating nephrotic syndrome, Front. Pharmacol. 12 (2022) 775745.
[21] R. Li, C.R. Shi, C.T. Wei, C. Wang, H.J. Du, R. Liu, X. Wang, Q. Hong, X.M. Chen, Fufang Shenhua tablet inhibits renal fibrosis by inhibiting PI3K/AKT, Phytomed 116 (2023) 154873.
[22] L.K. Chao, W.T. Chang, Y.W. Shih, J.S. Huang, Cinnamaldehyde impairs high glucose-induced hypertrophy in renal interstitial fibroblasts, Toxicol. Appl. Pharmacol. 244 (2010) 174–180.
[23] L.S. Gouveia Moreira, I.S. Costa Brum, D.V. Reis, L. Trugilho, T. Chermut, M. Esgalhado, L. Cardozo, P. Stenvinkel, P. Shiels, D. Mafra, Cinnamon: an aromatic condiment applicable to chronic kidney disease, Kidney Res. Clin. Pract. 42 (2023) 4–26.
[24] V.A. Bhattaram, U. Graefe, C. Kohlert, M. Veit, H. Derendorf, Pharmacokinetics and bioavailability of herbal medicinal products, Phytomed 9 (2002) 1–33.
[25] Y. He, Z.K. Zhou, W.J. Li, Y.Q. Zhang, R.Y. Shi, T. Li, Metabolic profiling and pharmacokinetic studies of Baihu-Guizhi decoction in rats by UFLC-Q-TOF-MS/MS and UHPLC-Q-TRAP-MS/MS, Chin. Med. 17 (2022) 117–130.
[26] H.F. Zhang, Yl Wang, C. Gao, Y.T. Gu, J. Huang, J.H. Wang, Z. Zhang, Salvianolic acid A attenuates kidney injury and inflammation by inhibiting NF-κB and p38 MAPK signaling pathways in 5/6 nephrectomized rats, Acta Pharmacol. Sin. 39 (2018) 1855–1864.
[27] J. Zhang, C.S. Wang, K. Kang, H.T. Liu, X.W. Liu, X.N. Jia, K.J. Yu, Loganin attenuates septic acute renal injury with the participation of AKT and Nrf2/HO-1 signaling pathways, Drug Des. Dev. Ther. 15 (2021) 501–513.
[28] X. Gao, Y. Liu, L. Wang, N. Sai, Y.X. Liu, J. Ni, Morroniside inhibits H_2O_2-induced podocyte apoptosis by downregulating NOX4 expression controlled by autophagy *in vitro*, Front. Pharmacol. 11 (2020) 533809.
[29] D.Q. Chen, L. Chen, Y. Guo, X.Q. Wu, T.T. Zhao, H.L. Zhao, H.J. Zhang, M.H. Yan, G.Q. Zhang, P. Li, Poricoic acid A suppresses renal fibroblast activation and interstitial fibrosis in UUO rats via upregulating Sirt3 and promoting β-catenin K49 deacetylation, Acta Pharmacol. Sin. 44 (2023) 1038–1050.
[30] Q. Li, Y. Ming, H. Jia, G. Wang, Poricoic acid A suppresses TGF-β1-induced renal fibrosis and proliferation via the PDGF-C, Smad3 and MAPK pathways, Exp. Ther. Med. 21 (2021) 289–296.
[31] A. Sharma, S. Sinha, N. Shrivastava, Apigenin and kaempferol as novel renoprotective agent against cisplatin-induced toxicity: an *in vitro* study, Exp. Ther. Med. 36 (2022) 6085–6090.
[32] Q.J. Wu, W. Li, J. Zhao, W. Sun, Q.Q. Yang, C. Chen, P. Xia, J.J. Zhu, Y.C. Zhou, G. S. Huang, C. Yong, M. Zheng, E.C. Zhou, K. Gao, Apigenin ameliorates doxorubicin-induced renal injury via inhibition of oxidative stress and inflammation, Biomed. Pharmacother. 137 (2021) 111308.
[33] Q. Zhou, K.W. Cheng, J. Gong, E. Li, M.F. Wang, Apigenin and its methylglyoxal-adduct inhibit advanced glycation end products-induced oxidative stress and inflammation in endothelial cells, Biochem. Pharmacol. 166 (2019) 231–241.
[34] L. Zhang, Y.Z. Zou, W.Y. Gong, Z.Q. Che, H.Q. Huang, Paeonol up-regulates CKIP-1 to resist high glucose-induced fibrosis in glomerular mesangial cells, Chin. Pharmacol. Bull. 5 (2018) 645–650.
[35] H. Zhou, Z.Z. Qiu, Z.H. Yu, L. Gao, J.M. He, Z.W. Zhang, Paeonol reverses promoting effect of the HOTAIR/miR-124/Notch1 axis on renal interstitial fibrosis in a rat model, J. Cell. Physiol. 234 (2019) 14351–14363.